Article:
Rawl, R., Ge, L., Lu, Z. et al. (2019) Ba8 MnNb6 O24: A model two-dimensional spin- 5/2 triangular lattice antiferromagnet. Physical Review Materials, 3 (5). 054412. ISSN: 2475-9953

https://doi.org/10.1103/physrevmaterials.3.054412

$Ba_8MnNb_6O_{24}$: A model two-dimensional spin-$\frac{5}{2}$ triangular lattice antiferromagnet

R. Rawl,[1] L. Ge,[2] Z. Lu,[3] Z. Evenson,[4] C. R. Dela Cruz,[5] Q. Huang,[1] M. Lee,[6,7] E. S. Choi,[7] M. Mourigal,[2] H. D. Zhou,[1,8,*] and J. Ma[8,9,†]

[1]*Department of Physics and Astronomy, University of Tennessee, Knoxville, Tennessee 37996, USA*
[2]*School of Physics, Georgia Institute of Technology, Atlanta, Georgia 30332, USA*
[3]*Helmholtz-Zentrum Berlin für Materialien und Energie, D-14109 Berlin, Germany*
[4]*Heinz Maier-Leibnitz Zentrum (MLZ) and Physik Department, Technische Universität München, Garching 85748, Germany*
[5]*Quantum Condensed Matter Division, Oak Ridge National Laboratory, Oak Ridge, Tennessee 37381, USA*
[6]*Department of Physics, Florida State University, Tallahassee, Florida 32306, USA*
[7]*National High Magnetic Field Laboratory, Florida State University, Tallahassee, Florida 32310, USA*
[8]*Key Laboratory of Artificial Structures and Quantum Control, School of Physics and Astronomy, Shanghai Jiao Tong University, Shanghai 200240, China*
[9]*Collaborative Innovation Center of Advanced Microstructures, Nanjing University, Nanjing, Jiangsu 210093, China*

(Received 24 January 2019; revised manuscript received 28 March 2019; published 28 May 2019)

We successfully synthesized and characterized the triangular lattice antiferromagnet $Ba_8MnNb_6O_{24}$, which comprises equilateral spin-$\frac{5}{2}$ Mn^{2+} triangular layers separated by six nonmagnetic Nb^{5+} layers. The detailed susceptibility, specific heat, elastic and inelastic neutron scattering measurements, and spin-wave theory simulation on this system reveal that it has a 120° ordering ground state below $T_N = 1.45$ K with in-plane nearest-neighbor exchange interaction ≈ 0.11 meV. While the large separation 18.9 Å between magnetic layers makes the interlayer exchange interaction virtually zero, our results suggest that a weak easy-plane anisotropy is the driving force for the $\mathbf{k}_m = (1/3, 1/3, 0)$ magnetic ordering. The magnetic properties of $Ba_8MnNb_6O_{24}$, along with its classical excitation spectra, contrast with the related triple perovskite $Ba_3MnNb_2O_9$, which shows easy-axis anisotropy, and the isostructural compound $Ba_8CoNb_6O_{24}$, in which the effective spin-$\frac{1}{2}$ Co^{2+} spins do not order down to 60 mK and in which the spin dynamics shows signs of strong quantum effects.

DOI: 10.1103/PhysRevMaterials.3.054412

I. INTRODUCTION

Truly two-dimensional (2D) lattices of interacting spins, including triangular, honeycomb, and kagome antiferromagnets, are of central interest to stabilize, explore, and understand exotic quantum states and their excitations [1–22]. However, the experimental realization of an ideal 2D magnetic system embedded in a bulk crystal is very difficult, since undesired factors such as lattice distortions, interplane interactions, and anisotropies are often present and transform the system of interest into, at best, a quasi-2D environment.

The design and synthesis of bulk materials with an ideal 2D magnetic lattice has been a challenge in the materials science community. Here, our strategy to achieve two-dimensionality is to insert nonmagnetic buffer layers between magnetic layers in a three-dimensional crystal structure. This idea has been applied to the perovskite structure (ABO_3) comprised of stacked triangular layers of B ions to yield triple perovskite structure ($A_3B'B_2O_9$). By having triangular layers of magnetic B′ ions separated by two triangular layers of nonmagnetic B ions, the interlayer distance gets increased and the interlayer interactions weakened. As a result, $A_3B'B_2O_9$ realizes ideal quasi-2D magnets for exploring exotic magnetic properties. Examples of such a triple perovskite structure are $Ba_3B'Nb_2O_9$ and $Ba_3B'Sb_2O_9$ ($B'^{2+} = Co^{2+}$, Ni^{2+}, and Mn^{2+} with spin number 1/2, 1, and 5/2, respectively) [14,15,20–25].

Among these materials, $Ba_3CoSb_2O_9$ is arguably the most interesting one stabilizing a one-third magnetization plateau as well as carrying anomalous zero-field magnetic excitations [14–19,26,27]. Proceeding from the triple perovskite structure, and with the strategy outlined above, we previously modified and expanded $Ba_3CoSb_2O_9$ to $Ba_8CoNb_6O_{24}$ with six layers of nonmagnetic Nb and a vacant layer between each layer of magnetic Co^{2+} ions [28,29]. In $Ba_3CoSb_2O_9$, the intraplane Co-Co distance is 5.86 Å and the interplane Co-Co distance is 7.23 Å, which yields an interlayer exchange interaction (J') around 5% the strength of the intralayer exchange interaction (J) [14–19,26,27]. Also present in $Ba_3CoSb_2O_9$ is a small easy-plane XXZ anisotropy (the ratio between the longitudinal and transverse exchange interactions is $\Delta \approx 0.9$). In contrast, $Ba_8CoNb_6O_{24}$ has a similar intralayer Co-Co distance of 5.79 Å, while the interlayer distances expand to 18.90 Å. This reduces the interplane interaction below detectable limits of susceptibility and specific-heat measurements and also removes any resolvable anisotropy, producing a virtually ideal 2D magnetic lattice with no ordering down to 60 mK, as our recent studies show. Moreover, its inelastic neutron scattering spectrum reveals a high-energy continuum also known as two-magnon scattering, which reflects the reduction of the ordered moment by quantum fluctuations. Therefore, $Ba_8CoNb_6O_{24}$ is a rare example of a spin-$\frac{1}{2}$ triangular-lattice Heisenberg antiferromagnet in the 2D limit [28,29].

*jma3@sjtu.edu.cn
†hzhou10@utk.edu

The successful reduction of J' and anisotropy in $Ba_8CoNb_6O_{24}$ calls for engineering a similar material with classical spins. In this paper, we report the synthesis and characterization of $Ba_8MnNb_6O_{24}$, which is isostructural to $Ba_8CoNb_6O_{24}$, but with a Mn^{2+} (spin-$\frac{5}{2}$) 2D triangular lattice. The detailed dc, ac susceptibility, specific heat, elastic, and inelastic neutron scattering measurements on this system reveal that it has a 120° ordering ground state below $T_N = 1.45$ K. The linear spin-wave simulation along with the inelastic neutron scattering (INS) spectra extract the antiferromagnetic nearest-neighbor exchange $J = 0.11$ meV. Unlike the related triple perovskite $Ba_3MnNb_2O_9$ that shows the easy-axis anisotropy [24], we suggest $Ba_8MnNb_6O_{24}$ could have a rather weak easy-plane anisotropy.

Our paper is organized as follows. Section II presents our experimental and theoretical methods. Section III presents the results of our thermomagnetic, diffraction, and inelastic neutron scattering characterizations of powder samples of $Ba_8MnNb_6O_{24}$. Section IV discusses and interprets our experimental results. Section V serves as a conclusion.

II. EXPERIMENT

Our polycrystalline sample of $Ba_8MnNb_6O_{24}$ was prepared by solid-state reaction. Stoichiometric amounts of $BaCO_3$, MnO, and Nb_2O_5 were mixed in agate mortars, compressed into pellets, and annealed for 20 h at temperatures of 1525 and 1600 °C under Ar atmosphere with intermediate mixing. High-resolution neutron powder diffraction (NPD) measurements were performed by a neutron powder diffractometer, HB2A, at the High Flux Isotope Reactor (HFIR), Oak Ridge National Laboratory (ORNL), Oak Ridge, TN. Around 3 g of powder was loaded in an Al-cylinder can and mounted in a close-cycled refrigerator. We used a neutron wavelength of $\lambda = 1.5405$ and 2.4127 Å with a collimation of 12′-open-6′. The NPD patterns were analyzed by the Rietveld refinement program FULLPROF [30]. Powder inelastic neutron scattering was measured using the cold neutron time-of-flight spectrometer (TOFTOF) at the Heinz Maier-Leibnitz Zentrum (MLZ), Munich, Germany. Around 6 g of powder was loaded in an Al cylindrical can mounted at the bottom of a dilution refrigerator. An incident neutron energy of $E_i = 3.27$ meV was used, which yielded an elastic energy resolution of 0.08 meV. The data were binned into steps of 0.015 Å and 0.015 meV. The dc magnetic susceptibility measurements were performed using a Quantum Design superconducting interference device (SQUID) magnetometer with an applied field of 0.5 T. The dc magnetization was performed on a vibrating sample system (VSM) at the National High Magnetic Field Laboratory (NHMFL), Tallahassee, FL.

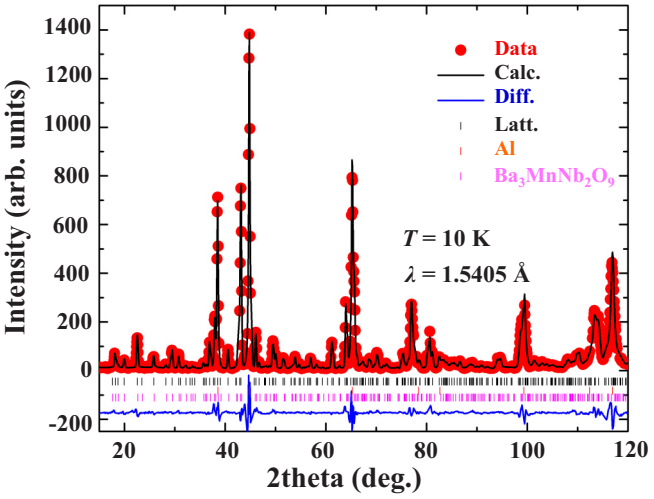

FIG. 1. Rietveld refinement of the neutron powder diffraction pattern of $Ba_8MnNb_6O_{24}$ measured at $T = 10$ K with $\lambda = 1.5405$ Å. Red circles are the measured intensity, the black line is the calculated intensity, and the blue line is the difference. Tick marks indicate lattice Bragg peak positions for $Ba_8MnNb_6O_{24}$ (upper black marks), the aluminum cab background (middle red marks), and ∼3% $Ba_3MnNb_2O_9$ impurity (lower magenta marks).

TABLE I. Structural parameters for $Ba_8MnNb_6O_{24}$ at 10 K (space group *P-3m1*) determined from refined NPD measurements.

Refinement	Atom	Site	x	y	z	Occupancy
	Ba1	2c	0	0	0.18732(84)	0.16666
$Ba_8MnNb_6O_{24}$	Ba2	2c	1/3	2/3	0.05867(120)	0.16666
rf-factor = 6.30	Ba3	2c	1/3	2/3	0.44997(89)	0.16666
Bragg R-factor = 7.28	Ba4	2c	1/3	2/3	0.68171(92)	0.16666
	Mn	1a	0	0	0	0.08333
	Nb1	2c	0	0	0.38767(61)	0.16667
	Nb2	2d	1/3	2/3	0.25790(82)	0.16667
	Nb3	2d	1/3	2/3	0.87545(74)	0.16667
	O1	6i	0.17214(116)	0.82786(116)	0.30799(46)	0.50
	O2	6i	0.16375(92)	0.83615(92)	0.57010(49)	0.50
	O3	6i	0.16731(117)	0.83259(117)	0.93445(58)	0.50
	O4	6i	0.49493(118)	0.50497(118)	0.18831(31)	0.50
Space group			Lattice parameters (Å)			
P-3*m*1			$a = b = 5.80701(6)$, $c = 18.94654(29)$		Overall B-factor = 0.156 (Å^2)	
Magnetic space group			Momentum			
P-1			$4.05(35)\mu_B$			

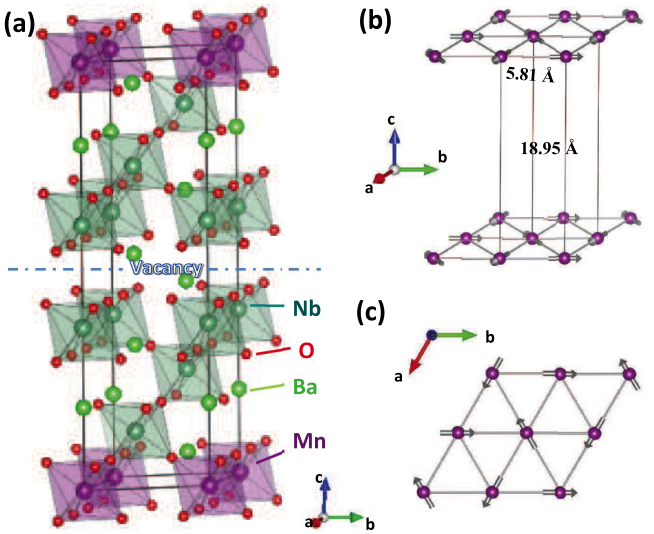

FIG. 2. (a) Stacked layer structure of $Ba_8MnNb_6O_{24}$. (b) Unit cell of $Ba_8MnNb_6O_{24}$ and spin structure of Mn^{2+} ions at zero field. (c) Triangular lattice composed of Mn^{2+} ions in the *ab* plane.

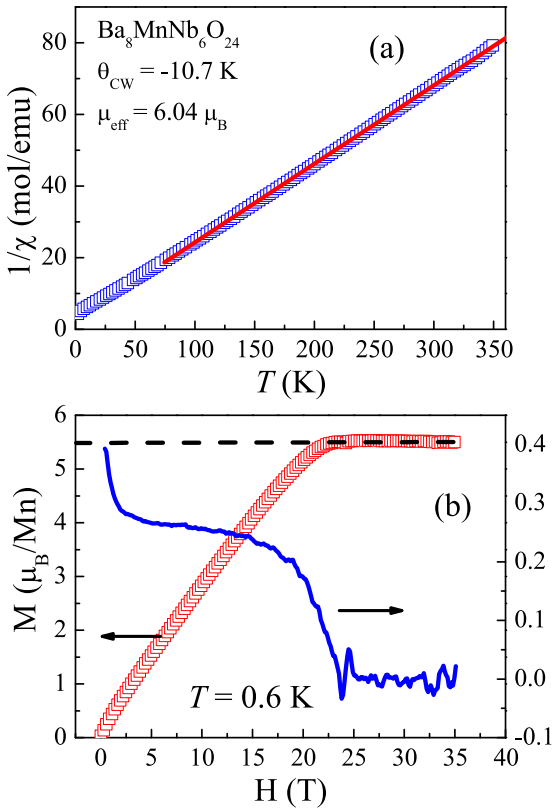

FIG. 3. (a) The inverse of the dc susceptibility (open squares) measured at a field of 0.5 T. The solid line is the Curie-Weiss fitting from 100 to 350 K. (b) The dc magnetization up to 35 T measured at 0.6 K, showing a saturation field ~22.5 T with a saturation moment of $5.50\mu_B/Mn^{2+}$. The solid line is the derivative of the magnetization.

The ac susceptibility measurements were taken using the conventional mutual inductance technique with a homemade setup [31]. The specific-heat data were obtained using a commercial physical property measurement system (PPMS, Quantum Design).

III. RESULTS

A. Lattice structure

Figure 1 shows the NPD pattern of $Ba_8MnNb_6O_{24}$ measured at $T = 10$ K with wavelength $\lambda = 1.5405$ Å. A Rietveld refinement yields a pure phase of the space group *P-3m1* with the lattice parameters of $a = 5.8070(1)$ Å and $c = 18.9465(3)$ Å. The details of the structural parameters are listed in Table I and confirm that $Ba_8MnNb_6O_{24}$ is isostructural to $Ba_8CoNb_6O_{24}$. No antisite disorder between Mn^{2+} and Nb^{5+} ions was observed, while ~3% $Ba_3MnNb_2O_9$ had been identified as the impurity. A crystallographic unit-cell [Fig. 2(a)] contains a vacant layer and *six layers* of nonmagnetic NbO_6 octahedral separating triangular layers of Mn^{2+} ions. While the intralayer Mn-Mn distance is around 5.81 Å, the interlayer Mn-Mn distance is as large as 18.91 Å [Fig. 2(b)]. This remarkable structure is expected to guarantee that the interlayer interaction of $Ba_8MnNb_6O_{24}$ is approaching the zero limit.

B. dc and ac susceptibility

Figure 3(a) reports the temperature dependence of the magnetic dc susceptibility χ of $Ba_8MnNb_6O_{24}$. No sign of magnetic ordering is observed down to 1.8 K, and a Curie-Weiss fit of the inverse dc susceptibility in the range of temperatures 100–350 K yields $\mu_{eff} = 6.04\mu_B$ and $\theta_W = -10.7$ K. The negative Weiss constant indicates overall antiferromagnetic exchange interactions, while the obtained effective magnetic moment agrees well with the value $5.93\mu_B$ expected for spin-only $S = 5/2$ magnetic moments [32]. Hereafter, we will consider the Hamiltonian of a triangular Heisenberg antiferromagnet,

$$\mathcal{H} = J \sum_{\langle i,j \rangle} \left(S_i^x S_j^x + S_i^y S_j^y + \Delta S_i^z S_j^z \right), \quad (1)$$

where $\langle i, j \rangle$ indicates the nearest neighbors and Δ indicates the potential easy-plane anisotropy which is not considered until Sec. III D. Considering $z = 6$ nearest-neighbour magnetic moments coupled with the Heisenberg exchange interaction J, mean-field theory yields $\theta_W = -zJS(S+1)/6k_B$, which corresponds to $J/k_B = -4/35\theta_{CW} = 1.22$ K for $Ba_8MnNb_6O_{24}$. The isothermal dc magnetization taken at $T = 0.6$ K is shown in Fig. 3(b) and yields a moment of $5.5\mu_B$ above the saturation magnetic field $\mu_0 H_s \approx 22.5$ T. The value of the saturated moment corresponds to a powder-averaged gyromagnetic ratio $g = 2.1$ for Mn^{2+} ion assuming $S = 5/2$. Therefore, the exchange interaction, $J = \frac{g\mu_B H_{sat} S^{-1}}{9} = 1.41$ K, from the saturated field agreed with the temperature-dependence measurement of magnetization. The field derivative of the magnetization shows no obvious valley or peak that would indicate possible spin-state transitions.

The ac susceptibility, χ_{ac}, measured down to 0.3 K at a frequency of 347 Hz was used to probe lower-temperature

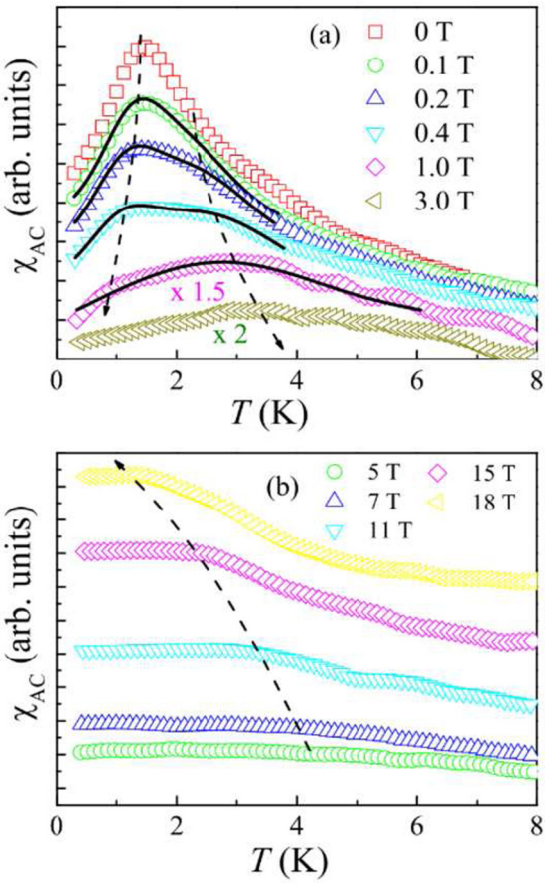

FIG. 4. The ac susceptibility for $Ba_8MnNb_6O_{24}$ under (a) low dc magnetic fields from 0 to 3.0 T. Fitting of the susceptibility with two Gaussian peaks is shown for several datasets (solid lines). (b) High dc magnetic fields from 5 to 18 T. The dashed arrowed lines are a guide to the eye to highlight the evolution of the peaks' position with increasing dc fields.

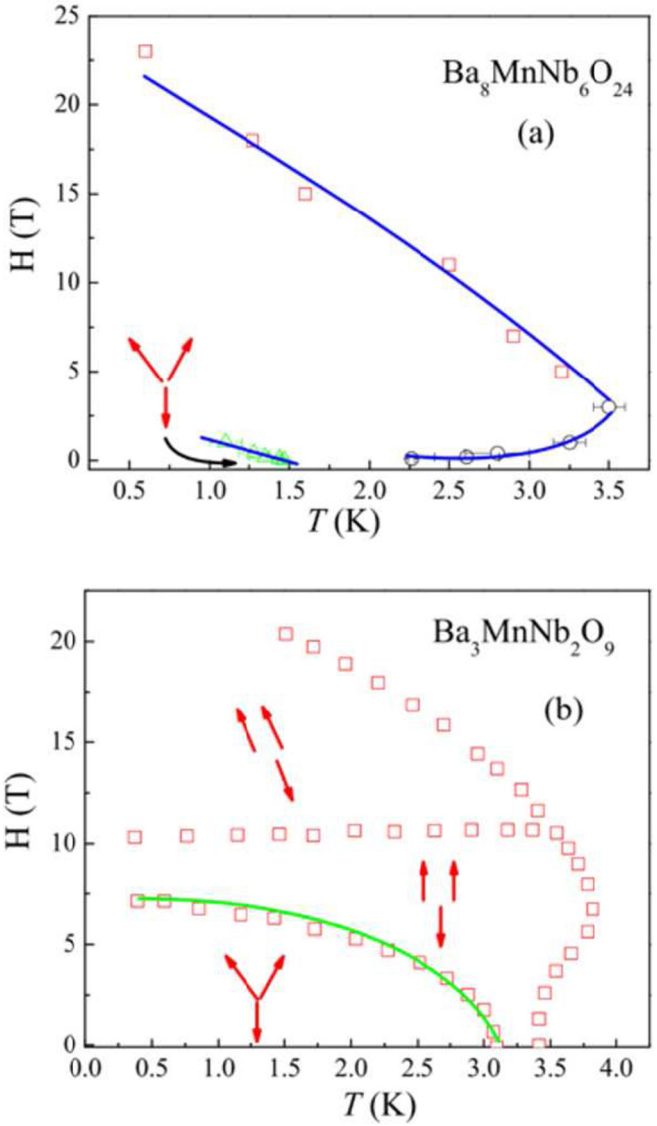

FIG. 5. The magnetic phase diagram (a) obtained for $Ba_8MnNb_6O_{24}$ in this work and (b) obtained for $Ba_3MnNb_2O_9$ in Ref. [24]. The drawn spin structures represent the canted 120°, up-up-down, and oblique phase, respectively.

magnetic properties of $Ba_8MnNb_6O_{24}$, as reported in Fig. 4. At zero dc field, χ_{ac} shows a sharp peak at 1.45 K, which indicates a transition to a long-range magnetic order. Upon application of a small dc magnetic field of 0.1 T, the peak broadens with a possible shoulder around 2.3 K. The susceptibility was fitted by two Gaussian peaks to determine the transitions of T_{N1} and T_{N2}, Fig. 4(a) (solid lines). A possible scenario to explain this behavior is that the single magnetic transition at zero dc field evolves into two transitions upon increasing the dc field, with T_{N1} referring to the low-temperature transition and T_{N2} the high-temperature one. With increasing dc field, Fig. 4(a), T_{N2} shifts to higher temperatures while T_{N1} shifts to lower temperatures and ultimately reaches below 0.3 K at 3.0 T. With even larger dc fields ($H > 3.0$ T), T_{N2} changes behavior from a maximum above 3.5 K around 4.0 T and shifts to lower temperatures with increasing dc field. Using the saturation field obtained from the dc magnetization and the T_N's obtained from the ac susceptibility data, we draw a magnetic phase diagram, Fig. 5(a), for $Ba_8MnNb_6O_{24}$ and compare it to recent results for $Ba_3MnNb_2O_9$ [24]. A more detailed discussion of this phase diagram will be presented below.

C. Specific heat

In Fig. 6(a) we show the specific heat, C_p, of $Ba_8MnNb_6O_{24}$ measured in magnetic fields of 0, 7, and 14 T. At zero field, C_p shows a broad peak around 4 K but no significant feature matching the kink observed around 1.45 K in the temperature dependence of the ac susceptibility. Moreover, the data show a sharp increase below 200 mK, which we ascribed to the nuclear Schottky anomaly of the Mn ions, since the naturally abundant 55Mn has nuclear spin $\frac{5}{2}$. This can also explain why the upturn shifts to higher temperatures with higher magnetic fields, because the magnetic ordered moment increases with the magnetic field and hence opens up the nuclear spin levels through the hyperfine coupling, which leads to the transition at higher temperatures. With increasing fields, the broad peak is somewhat suppressed. We isolate the magnetic contribution to the specific heat, (C_m), by

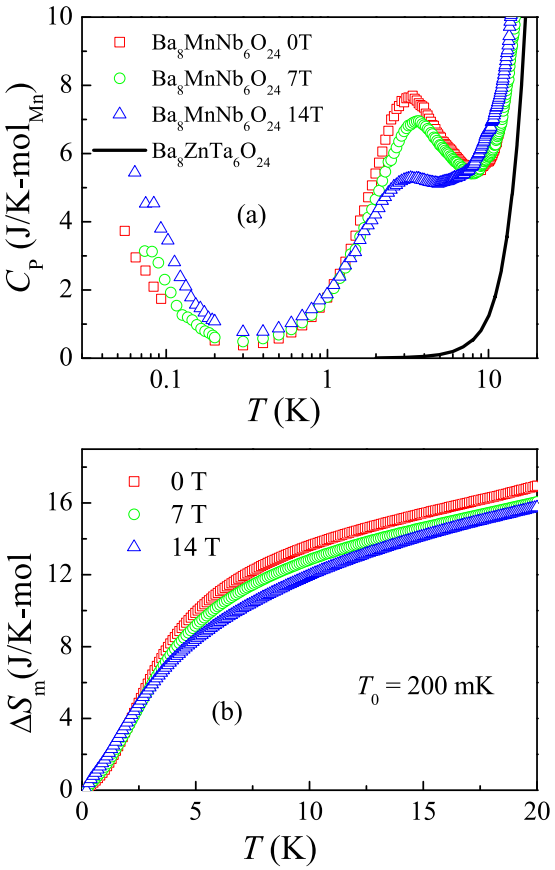

FIG. 6. (a) The specific heat, C_p, of $Ba_8MnNb_6O_{24}$ at 0, 7.0, and 14.0 T, and nonmagnetic analog $Ba_8ZnTa_6O_{24}$ (black line) to expose the lattice contribution. (b) Magnetic entropy change calculated from the integral of C_p/T with lattice subtracted starting at 200 mK.

subtracting the specific heat of the isostructural nonmagnetic compound $Ba_8ZnTa_6O_{24}$. This yields the magnetic entropy change, ΔS_m, calculated by integrating C_m/T. For simplicity, we did not subtract the nuclear Schottky anomaly from the data but performed the integration from 200 mK since at this temperature the C_p is already rather small. The obtained ΔS_m is around 16 J/mol K, a value near to the ideal value for $S = 5/2$, which is $R\ln(6) = 14.9$ J/mol K, with R as a gas constant.

D. Magnetic structure and excitations

In Fig. 7 we show the NPD pattern of $Ba_8MnNb_6O_{24}$ measured at 0.3 K with wavelength $\lambda = 2.4127$ Å. The data reveal the presence of magnetic Bragg peaks that can be indexed by $\mathbf{Q} = \boldsymbol{\tau} + \mathbf{k}_m$, where $\boldsymbol{\tau}$ is a reciprocal-lattice vector and $\mathbf{k}_m = (1/3, 1/3, 0)$. In the inset of Fig. 7, we highlight the difference between the 0.3 and 10.0 K data, which reveals the details of these magnetic Bragg peaks. The refined magnetic structure for the above propagation vector $\mathbf{k}_m$ is shown in Fig. 1(c): it corresponds to a 120° spin-structure in the *ab* plane with spins arranged in a collinear ferromagnetic arrangement between nearest-neighbor layers. The refined ordered moment is $4.6(1)\mu_B$ for each Mn^{2+} ion. Due to the small number of sizable magnetic Bragg peaks, the refinement

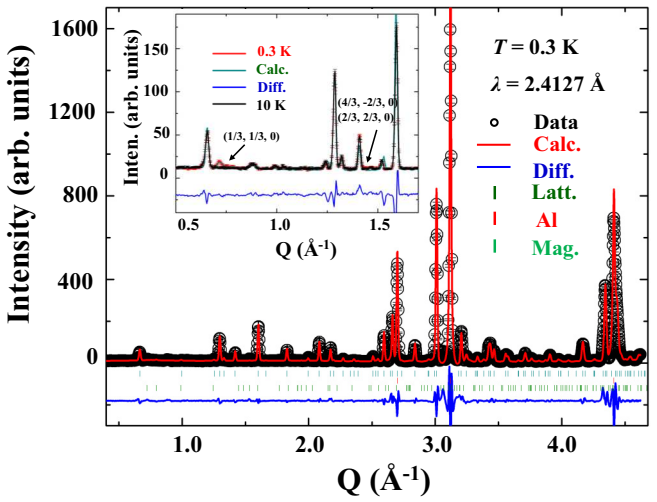

FIG. 7. Rietveld refinement of the neutron powder diffraction pattern measured at $T = 0.3$ K with $\lambda = 2.4127$ Å for $Ba_8MnNb_6O_{24}$. Black circles are the measured intensity, the red line is the calculated intensity, and the blue line is the difference. Tick marks are the lattice Bragg peak and aluminum and magnetic Bragg peak positions, from top to bottom, respectively. Inset: Highlight of the difference between the 0.3 and 10 K neutron powder diffraction patterns to show the magnetic Bragg peak positions.

cannot reveal whether the spins lie in the *ab* plane or in a plane containing the *c* axis (an easy-axis type 120° structure).

Figure 8 shows the powder INS spectra of $Ba_8MnNb_6O_{24}$ measured at 10, 4.0, 1.5, 0.4, and 0.05 K, respectively. The INS intensity as a function of momentum transfer Q and energy transfer E allows us to track the development of magnetic correlations upon lowering T. At high temperatures such as 10 and 4 K, the INS intensity shows a clear short-range magnetic signal with a momentum dependence peaked at $Q \approx 0.7$ Å^{-1}. Upon decreasing temperature and approaching T_N (1.45 K), sharper ridges of intensity emerge from $Q \approx 0.7$ Å^{-1} with less intense repetitions at 1.5 and 2.0 Å^{-1}, in perfect agreement with the powder-diffraction results. The energy dependence of the main signal reveals gapless excitations extending up to 1.0 meV. These features change very little below T_N from 0.4 to 0.05 K. This further confirms the occurrence of a well-correlated magnetic state below 1.0 K, consistent with long-range magnetic order.

To model the dynamic magnetic correlations in the ordered state, we resort to linear spin-wave theory at zero temperature [33]. We use a canonical Heisenberg Hamiltonian [Eq. (1)] with the 120° magnetic structure as the ground state. Due to the powder averaging effect, information about possible exchange anisotropies, which we expect to be relatively small, cannot be accurately extracted from the INS data and therefore are not considered here. The best match between the experimental data measured at $T = 0.05$ K and the simulation, Fig. 8(f), is achieved with the nearest-neighbor exchange interaction $J = 0.11$ meV (or 1.28 K). This value is consistent with the $J = 1.22$ K calculated from the Curie-Weiss temperature. As shown in Figs. 8(e) and 8(f), the calculated spectrum reproduces the main features of the experimental data, such

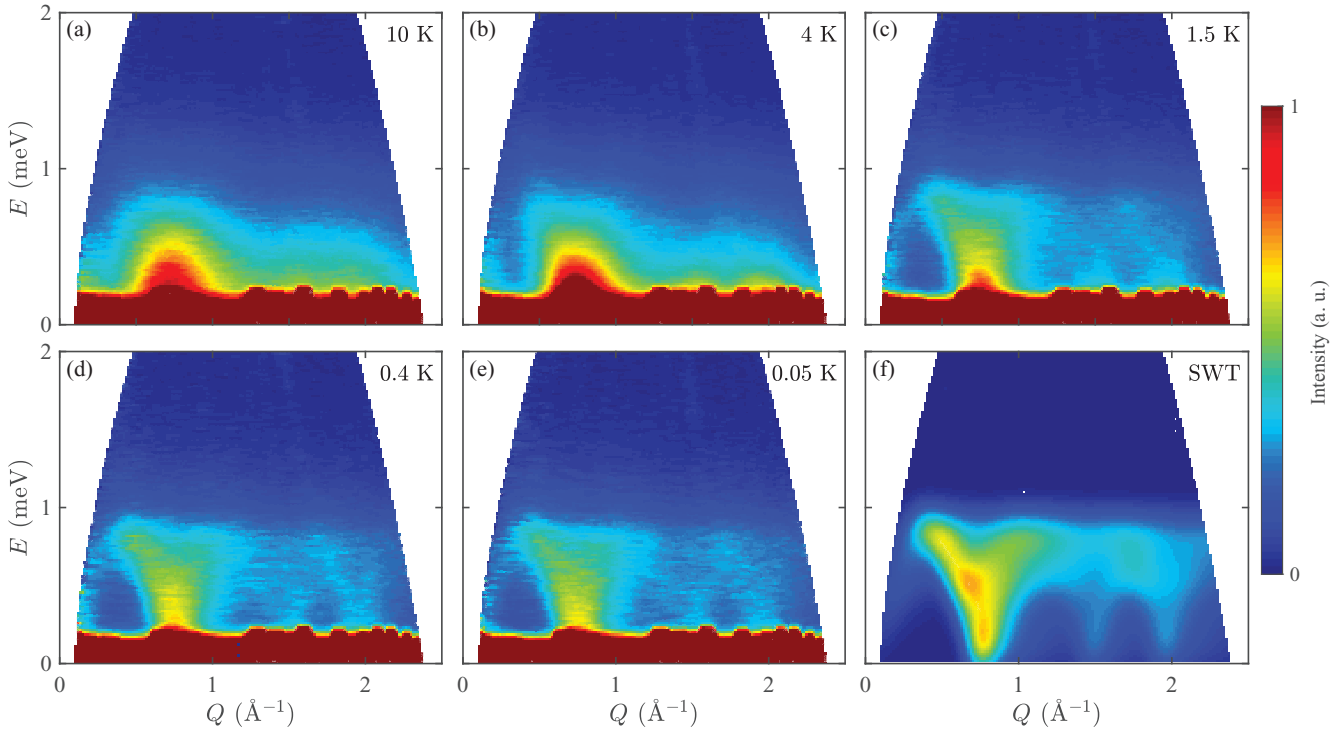

FIG. 8. (a)–(e) Powder inelastic neutron scattering spectra for $Ba_8MnNb_6O_{24}$ measured at nominal temperatures of 10, 4, 1.5, 0.4, and 0.05 K, respectively. (f) The neutron scattering intensity calculated for $J = 0.11$ meV using linear spin-wave theory.

as the positions of the zone centers and the bandwidth of the magnetic excitations. A more detailed illustration of the good match between experiment and our model is evident in E-integrated [Fig. 9(a)] and Q-integrated [Fig. 9(b)] cuts. We may also estimate the upper bound of the easy-plane anisotropy Δ from the INS data. Although such anisotropy does not gap the entire spin-wave dispersion relation in the Brillouin zone, there will be major intensity shifted up in the calculated spin dynamical structure factor at the ordering wave vector. This shift is essentially the energy gap of the out-of-plane mode. Within the linear spin-wave theory, the gap $\Delta\varepsilon$ is proportional to

$$\Delta\varepsilon = 3JS\sqrt{3(1-\Delta)/2}. \quad (2)$$

Meanwhile, the inelastic neutron scattering data we obtained have an incoherent elastic line that extends to roughly 0.2 meV. Therefore, we cannot resolve any potential gap if it is smaller than that. Now we just plug the values $J = 0.11$ meV, $S = 5/2$ into the above equation. We can obtain that $\Delta > 0.96$.

IV. DISCUSSION

A noteworthy feature of $Ba_8MnNb_6O_{24}$ is that the heat-capacity C_p shows no clear sign of long-range magnetic ordering but a broad peak around 4 K. Previous quantum Monte Carlo studies on quasi-2D antiferromagnetic Heisenberg models have shown that the onset of long-range magnetic ordering is accompanied with a sharp peak in C_p even for interlayer exchange interactions as small as $J'/J = 2 \times 10^{-4}$; see Ref. [34]. Upon further decreasing the interlayer coupling, the sharp peak disappears and only a broad peak remains. Therefore, we believe the sole broad peak in C_p hints at the almost ideal two-dimensional nature of magnetism in $Ba_8MnNb_6O_{24}$. At the same time, the broad peak indicates that the short-ranged spin correlations have already developed at temperatures higher than T_N. This is consistent with the INS observation, which shows that broad magnetic signals have already developed at as high as 10 K.

In spite of its almost ideal two-dimensional magnetism, $Ba_8MnNb_6O_{24}$ still appears to order at $T_N = 1.45$ K with a 120° ordering structure as confirmed by the ac susceptibility and neutron diffraction experiments. Since T_N increases logarithmically in the interlayer interaction or in the exchange anisotropy [35–41], we conjecture that the magnetic transition of $Ba_8MnNb_6O_{24}$ is most likely driven by an easy-plane anisotropy.

It is instructive to compare the magnetic properties of $Ba_8MnNb_6O_{24}$ with those of the related quasi-2D compound $Ba_3MnNb_2O_9$. For this purpose, the magnetic phase diagram for $Ba_3MnNb_2O_9$ is reproduced in Fig. 5(b). The major differences between these two phase diagrams are as follows. First, a two-step transition at $T_{N1} = 3.4$ K and $T_{N2} = 3.0$ K occurs in $Ba_3MnNb_2O_9$, which indicates its easy-axis anisotropy. This is not only the normal behavior for Mn^{2+} ions on octahedral sites as for $Rb_4Mn(MoO_4)_3$ [42], but also for the distorted triangular lattice in $A_3NiNb_2O_9$ [43] and $NaCrO_2$ ($NiGa_2S_4$) [44]. For some special case, the TLAF could exhibit easy-plane anisotropy. For example, the recently studied TLAF $Ba_2La_2MnW_2O_{12}$ shows a single-step transition, in which the competition between the antiferromagnetic Mn-O-O-Mn and ferromagnetic Mn-O-W-O-Mn could be the reason for the easy-plane anisotropy. In contrast, $Ba_8MnNb_6O_{24}$, potentially with a weak easy-plane anisotropy with transferring from one

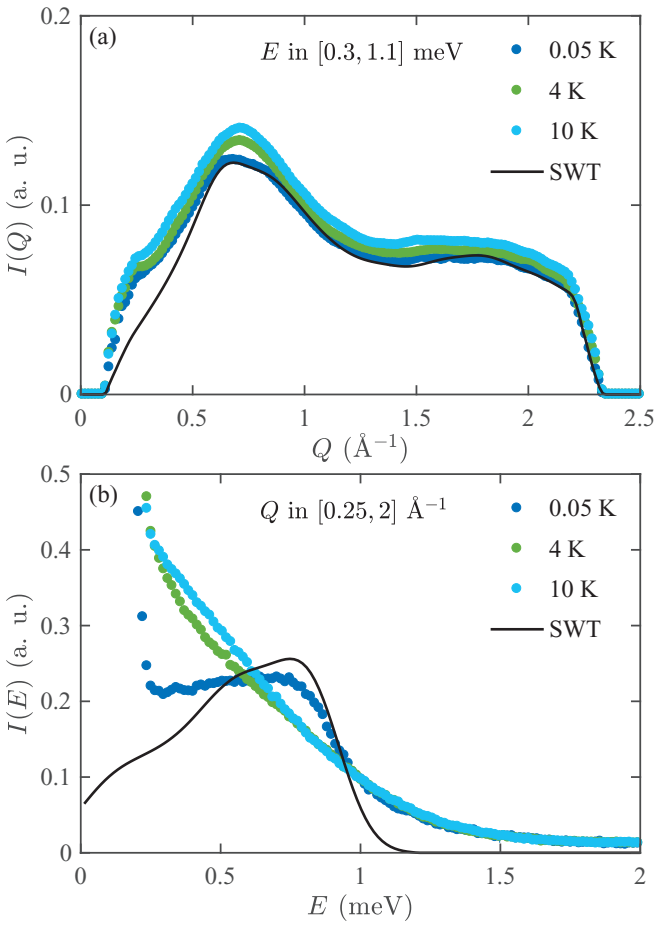

FIG. 9. Comparisons between experiment (dots) and linear spin-wave theory (black line) as energy-integrated ($0.3 \leqslant E \leqslant 1.1$ meV) and momentum-integrated ($0.25 \leqslant Q \leqslant 2$ Å^{-1}) cuts, respectively.

magnetic transition at 0 T to two transitions at very low field (0.1 T), sits closer to the limit of Heisenberg spins. Second, the magnetic phase diagram for $Ba_3MnNb_2O_9$ evolves from the zero-field 120° ordering to canted 120° ordering, UUD phase, and then oblique phase with increasing applied field, while there is no indication for the existence of the UUD phase in $Ba_8MnNb_6O_{24}$. Whether this disappearance of UUD phase is intrinsically related to dimensional reduction in $Ba_8MnNb_6O_{24}$ or is extrinsic due to the polycrystalline sample nature (in which the powder average effect smears the phase boundaries) needs to be clarified by more studies on putative single crystalline samples in the future.

Finally, we compare $Ba_8MnNb_6O_{24}$ with $Ba_8CoNb_6O_{24}$, where the main difference lies in the spin quantum number. With $S = 1/2$ magnetic moments, $Ba_8CoNb_6O_{24}$ is subject to stronger quantum fluctuations and thus exhibits no long-range magnetic order down to $T = 60$ mK and calls for $1/S$ spin-wave theory to model its magnetic excitations. Meanwhile, $Ba_8MnNb_6O_{24}$, with $S = 5/2$, is essentially in the classical limit and the resulting spin dynamics are well described by linear spin-wave theory without considering any form of magnon-magnon interactions. On top of quantum effects, thermal fluctuations should play an influential role in both systems. Therefore, $Ba_8MnNb_6O_{24}$, free from strong quantum fluctuations, may serve as a good candidate to investigate the role of thermal fluctuations.

V. CONCLUSION

We presented a detailed experimental study of the triangular lattice antiferromagnet $Ba_8MnNb_6O_{24}$ with $S = 5/2$ Mn^{2+} ions forming equilateral triangular lattices. Our results reveal that despite the almost ideally 2D nature of the magnetism and the likely vanishing interlayer interaction, long-range magnetic order develops at $T_N = 1.45$ K. Specific-heat measurements along with an inelastic neutron scattering study show that short-ranged spin correlations are well formed at a temperature as high as $T = 10$ K. Linear spin-wave theory simulations yield a nearest-neighbor interaction around 0.11 meV, in good agreement with an estimate from magnetic susceptibility measurements. By comparing with the related triple-perovskite $Ba_3MnNb_2O_9$ and the isostructural $Ba_8CoNb_6O_{24}$ with effective spin-$\frac{1}{2}$ Co^{2+} ions, we elucidated the subtle role played by the quantum spin number and putative weak anisotropies to produce long-range magnetic ordering in the 2D triangular lattice Heisenberg antiferromagnet $Ba_8MnNb_6O_{24}$.

ACKNOWLEDGMENTS

J.M. gratefully acknowledges the support from the Chinese Spallation Neutron Source (CSNS) User Special Grant, the NSF China (11774223), and the Ministry of Science and Technology of China (2016YFA0300500). R.R., Q.H., and H.D.Z. gratefully acknowledge the support from NSF-DMR through Award No. DMR-1350002. The work at Georgia Tech (L.G. and M.M.) was supported by the National Science Foundation through Grant No. NSF-DMR-1750186. This research used resources at the High Flux Isotope Reactor, a DOE Office of Science User Facility operated by the Oak Ridge National Laboratory. A portion of this work was performed at the NHMFL, which is supported by National Science Foundation Cooperative Agreement No. DMR-1157490 and the State of Florida. E.S.C. and M.L. acknowledge the support from NSF-DMR-1309146.

[1] Y. Li, G. Chen, W. Tong, L. Pi, J. Liu, Z. Yang, X. Wang, and Q. Zhang, Phys. Rev. Lett. **115**, 167203 (2015).

[2] Y. Shen, Y. D. Li, H. Wo, Y. Li, S. Shen, B. Pan, Q. Wang, H. C. Walker, P. Steffens, M. Boehm, Y. Hao, D. L. Quintero-Castro, L. W. Harriger, M. D. Frontzek, L. Hao, S. Meng, Q. Zhange, G. Chen, and J. Zhao, Nature (London) **540**, 559 (2016).

[3] J. A. M. Paddison, M. Daum, Z. Dun, G. Ehlers, Y. Liu, M. B. Stone, H. Zhou, and M. Mourigal, Nat. Phys. **13**, 117 (2016).

[4] A. Banerjee, C. A. Bridges, J.-Q. Yan, A. A. Aczel, L. Li, M. B. Stone, G. E. Granroth, M. D. Lumsden, Y. Yiu, J. Knolle, S. Bhattacharjee, D. L. Kovrizhin, R. Moessner, D. A. Tennant, D. G. Mandrus, and S. E. Nagler, Nat. Mater. **15**, 733 (2016).

[5] A. Banerjee, J.-Q. Yan, J. Knolle, C. A. Bridges, M. B. Stone, M. D. Lumsden, D. G. Mandrus, D. A. Tennant, R. Moessner, and S. E. Nagler, Science **356**, 1055 (2017).

[6] A. Little, L. Wu, P. Lampen-Kelley, A. Banerjee, S. Patankar, D. Rees, C. A. Bridges, J.-Q. Yan, D. Mandrus, S. E. Nagler, and J. Orenstein, Phys. Rev. Lett. **119**, 227201 (2017).

[7] T. H. Han, J. S. Helton, S. Chu, D. G. Nocera, J. A. Rodriguez-Rivera, C. Broholm, and Y. S. Lee, Nat. Phys. **492**, 406 (2012).

[8] M. Fu, T. Imai, T. H. Han, and Y. S. Lee, Science **350**, 655 (2015).

[9] J. S. Helton, K. Matan, M. P. Shores, E. A. Nytko, B. M. Bartlett, Y. Yoshida, Y. Takano, A. Suslov, Y. Qiu, J.-H. Chung, D. G. Nocera, and Y. S. Lee, Phys. Rev. Lett. **98**, 107204 (2007).

[10] Z. L. Dun, J. Trinh, K. Li, M. Lee, K. W. Chen, R. Baumbach, Y. F. Hu, Y. X. Wang, E. S. Choi, B. S. Shastry, A. P. Ramirez, and H. D. Zhou, Phys. Rev. Lett. **116**, 157201 (2016).

[11] Z. L. Dun, J. Trinh, M. Lee, E. S. Choi, K. Li, Y. F. Hu, Y. X. Wang, N. Blanc, A. P. Ramirez, and H. D. Zhou, Phys. Rev. B **95**, 104439 (2017).

[12] T. Ono, H. Tanaka, H. Aruga Katori, F. Ishikawa, H. Mitamura, and T. Goto, Phys. Rev. B **67**, 104431 (2003).

[13] N. A. Fortune, S. T. Hannahs, Y. Yoshida, T. E. Sherline, T. Ono, H. Tanaka, and Y. Takano, Phys. Rev. Lett. **102**, 257201 (2009).

[14] Y. Shirata, H. Tanaka, A. Matsuo, and K. Kindo, Phys. Rev. Lett. **108**, 057205 (2012).

[15] T. Susuki, N. Kurita, T. Tanaka, H. Nojiri, A. Matsuo, K. Kindo, and H. Tanaka, Phys. Rev. Lett. **110**, 267201 (2013).

[16] H. D. Zhou, C. Xu, A. M. Hallas, H. J. Silverstein, C. R. Wiebe, I. Umegaki, J. Q. Yan, T. P. Murphy, J. H. Park, Y. Qiu, J. R. D. Copley, J. S. Gardner, and Y. Takano, Phys. Rev. Lett. **109**, 267206 (2012).

[17] G. Quirion, M. Lapointe-Major, M. Poirier, J. A. Quilliam, Z. L. Dun, and H. D. Zhou, Phys. Rev. B **92**, 014414 (2015).

[18] G. Koutroulakis, T. Zhou, Y. Kamiya, J. D. Thompson, H. D. Zhou, C. D. Batista, and S. E. Brown, Phys. Rev. B **91**, 024410 (2015).

[19] J. Ma, Y. Kamiya, T. Hong, H. B. Cao, G. Ehlers, W. Tian, C. D. Batista, Z. L. Dun, H. D. Zhou, and M. Matsuda, Phys. Rev. Lett. **116**, 087201 (2016).

[20] Y. Shirata, H. Tanaka, T. Ono, A. Matsuo, K. Kindo, and H. Nakano, J. Phys. Soc. Jpn. **80**, 093702 (2011).

[21] M. Lee, J. Hwang, E. S. Choi, J. Ma, C. R. Dela Cruz, M. Zhu, X. Ke, Z. L. Dun, and H. D. Zhou, Phys. Rev. B **89**, 104420 (2014).

[22] K. Yokota, N. Kurita, and H. Tanaka, Phys. Rev. B **90**, 014403 (2014).

[23] Y. Doi, Y. Hinatsu, and K. Ohoyama, J. Phys. Condens. Matter **16**, 8923 (2004).

[24] M. Lee, E. S. Choi, X. Huang, J. Ma, C. R. Dela Cruz, M. Matsuda, W. Tian, Z. L. Dun, S. Dong, and H. D. Zhou, Phys. Rev. B **90**, 224402 (2014).

[25] J. Hwang, E. S. Choi, F. Ye, C. R. Dela Cruz, Y. Xin, H. D. Zhou, and P. Schlottmann, Phys. Rev. Lett. **109**, 257205 (2012).

[26] S. Ito, N. Kurita, H. Tanaka, S. Ohira-Kawamura, K. Nakajima, S. Itoh, K. Kuwahara, and K. Kakurai, Nat. Commun. **8**, 235 (2017).

[27] Y. Kamiya, L. Ge, T. Hong, Y. Qiu, D. L. Quintero-Castro, Z. Lu, H. B. Cao, M. Matsuda, E. S. Choi, C. D. Batista, M. Mourigal, H. D. Zhou, and J. Ma, Nat. Commun. **9**, 2666 (2018).

[28] R. Rawl, L. Ge, H. Agrawal, Y. Kamiya, C. R. Dela Cruz, N. P. Butch, X. F. Sun, M. Lee, E. S. Choi, J. Oitmaa, C. D. Batista, M. Mourigal, H. D. Zhou, and J. Ma, Phys. Rev. B **95**, 060412(R) (2017).

[29] Y. Cui, J. Dai, P. Zhou, P. S. Wang, T. R. Li, W. H. Song, L. Ma, Z. Zhang, S. Y. Li, G. M. Luke, B. Normand, T. Xiang, and W. Yu, Phys. Rev. Mater. **2**, 044403 (2018).

[30] J. Rodriguez-Carvajal, Physica B **192**, 55 (1993).

[31] Z. L. Dun, M. Lee, E. S. Choi, A. M. Hallas, C. R. Wiebe, J. S. Gardner, E. Arrighi, R. S. Freitas, A. M. Arevalo-Lopez, J. P. Attfield, H. D. Zhou, and J. G. Cheng, Phys. Rev. B **89**, 064401 (2014).

[32] G. A. Parks and S. Akhtar, Am. Mineral. **53**, 406 (1968).

[33] S. Toth and B. Lake, J. Phys.: Condens. Matter **27**, 166002 (2015).

[34] P. Sengupta, A. W. Sandvik, and R. R. P. Singh, Phys. Rev. B **68**, 094423 (2003).

[35] K. Hirakawa, J. Appl. Phys. **53**, 1893 (1982).

[36] A. Cuccoli, T. Roscilde, R. Vaia, and P. Verrucchi, Phys. Rev. Lett. **90**, 167205 (2003).

[37] S. Miyashita and H. Kawamura, J. Phys. Soc. Jpn. **54**, 3385 (1985).

[38] W. Stephan and B. W. Southern, Phys. Rev. B **61**, 11514 (2000).

[39] S. Fujimoto, Phys. Rev. B **73**, 184401 (2006).

[40] H. Kawamura and S. Miyashita, J. Phys. Soc. Jpn. **53**, 4138 (1984).

[41] H. Kawamura and S. Miyashita, J. Phys. Soc. Jpn. **54**, 4530 (1985).

[42] R. Ishii, S. Tanaka, K. Onuma, Y. Nambu, M. Tokunaga, T. Sakakibara, N. Kawashima, Y. Maeno, C. Broholm, D. P. Gautreaux, J. Y. Chan, and S. Nakatsuji, Europhys. Lett. **94**, 17001 (2011).

[43] Z. Lu, L. Ge, G. Wang, M. Russina, G. Guenther, C. R. dela Cruz, R. Sinclair, H. D. Zhou, and J. Ma, Phys. Rev. B **98**, 094412 (2018).

[44] H. Kawamura, A. Yamamoto, and T.Okubo, J. Phys. Soc. Jpn. **79**, 023701 (2010).